Food Chemistry: X 20 (2023) 101020

Contents lists available at ScienceDirect

Food Chemistry: X

journal homepage: www.sciencedirect.com/journal/food-chemistry-x

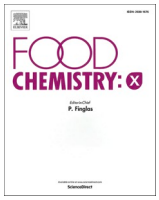

The influence of different gums compared with surfactants as encapsulating stabilizers on the thermal, storage, and low-pH stability of chlorophyllin

Hamed Hosseini [a], Vahid Pasban Noghabi [b], Hamed Saberian [c], Seid Mahdi Jafari [d,e,*]

[a] Food Additives Research Department, Food Science and Technology Research Institute, Iranian Academic Centre for Education, Culture and Research (ACECR), Khorasan Razavi Branch, Mashhad, Iran
[b] Department of Food Science and Technology, ACECR Kashmar Higher Education Institute, Kashmar, Iran
[c] Department of Agro-industrial Waste Processing, Academic Center for Education, Culture and Research (ACECR), IUT Branch, Isfahan, Iran
[d] Department of Food Materials and Process Design Engineering, Gorgan University of Agricultural Science and Natural Resources, Gorgan, Iran
[e] Halal Research Center of IRI, Iran Food and Drug Administration, Ministry of Health and Medical Education, Tehran, Iran

ARTICLE INFO

Keywords:
Chlorophyllin
Low pH stability
Pasteurization
Zeta-potential
Hydrocolloids

ABSTRACT

Sodium copper chlorophyllin (SCC), with a higher stability and water solubility than chlorophyll, has limited applications in acidic products due to precipitation. We investigated the effect of pectin (PE), carboxymethyl cellulose (CMC), xanthan gum (XG), carrageenan gum (CG), gellan gum (GG), tragacanth gum (TG), gum Arabic (GA), and polysorbate 80 (PS80) on SCC stability in acidic model solutions (pH = 3.5). These stabilizers led to a significant reduction in particle size and zeta-potential compared to control sample. GA (33.3:1), PE (8:1), CMC (4:1), XG (1.33:1), and PS80 (0.67:1) stabilized SCC in acidic systems for 28 days. The FTIR analysis showed that mainly electrostatic and hydrogen bonds between SCC and stabilizers led to a substantial decline in particle size, improving SCC distribution and stability within acidic environment. Thus, XG and CMC could be effectively used for SCC stabilization under acidic solutions where applying PS80 surfactant is a health concern.

1. Introduction

Natural pigments are a very good alternative to the synthetic ones as their application in foods and drinks is increasing. However, their technical disadvantages, such as relatively low stability compared to synthetic colors have presented some challenges. Chlorophyll is a natural green pigment abundant in fruits and vegetables and is extracted from edible green plants such as grass, alfalfa, nettle, as well as leaves of some plants using safe solvents. This pigment is stable in nature, but when extracted from plant tissues, it is degraded by light, heat, oxygen, acids, and enzymes. Upon pheophytization, the color change occurs from green chlorophyll to brown or gray-green (Koca et al., 2007). Some derivatives have been prepared to stabilize chlorophyll. The main advantage of sodium copper chlorophyllin (SCC) complex compared to chlorophyll is its good stability in environmental conditions, as well as its water solubility. However, SCC precipitates under acidic conditions which is the main challenge for this pigment in acidic products, especially drinks, jellies, and pastilles (Tumolo and Lanfer-Marquez, 2012).

Polyethylene sorbitol ester, known as polysorbate 80/Tween 80 (PS80), consists of ethylene oxide (hydrophilic) and the fatty acid chain (hydrophobic) units, providing its amphiphilic characteristics as a synthetic nonionic surfactant. It is broadly used as a nonionic surfactant to enhance the solubility and distribution of substances. Frost and Saleeb (1999) used PS80 to produce acid-resistant SCC (pH $\leq$ 4) in a PS80-to-SCC ratio of 0.2–5:1–3. However, considering its health concerns (Schwartzberg and Navari, 2018), it could be worth to substitute PS80 with safe ingredients such as biopolymers. Hydrocolloids also appear to have a similar effect on SCC, enclosing them, spacing them apart, and preventing them against precipitation. Owing to functional groups (mainly COOH) on the structure of gums, they have been found to be good stabilizer agents, contributing to electrostatic interactions and forming complexes with metal ions (Roque et al., 2009; Shaddel et al., 2018; Cai et al., 2020). In this regard, Selig et al. (2020) investigated the effect of sodium alginate and xanthan gum (XG) on the stability of SCC pigment at pH = 3 and 5; they observed that both hydrocolloids could stabilize the green color in acidic conditions and at refrigerator temperature; however, color change to olive green was also reported in a solution containing XG. They suggested XG as the most desirable

* Corresponding author at: Department of Food Materials and Process Design Engineering, Gorgan University of Agricultural Science and Natural Resources, Gorgan, Iran.
E-mail address: smjafari@gau.ac.ir (S.M. Jafari).

https://doi.org/10.1016/j.fochx.2023.101020
Received 29 June 2023; Received in revised form 8 November 2023; Accepted 19 November 2023
Available online 20 November 2023

stabilizer.

Sodium carboxymethyl cellulose (CMC) is a natural polymer synthesized from cellulose. The molecular structure of this anionic biopolymer is composed of the hydrophobic polysaccharide backbone (β-(1–4) linked D-glucose units) containing hydrophilic carboxyl groups with different degrees of substitution. Owing to hydrophilic carboxyl groups, CMC shows excellent electrical and water retention properties; thus, it is widely used as a thickener and stabilizer agent in the food industry (Mazuki et al., 2020). Gum Arabic (GA) –as a hetero-polysaccharide– is a covalently linked mixture of high molecular weight glycoproteins in a low amount and a higher content of arabinogalactan, as a highly branched polysaccharide with a lower molecular weight. The remarkable features of GA, namely surface-active and rheological properties make this biopolymer suitable to be used as a hydrocolloid emulsifier, stabilizer, and thickening agent in different industries (Roque et al., 2009). Pectin (PE) –a polysaccharide rich in D-galacturonic acid (GalA)– is mainly composed of homogalacturonans, consisting of a linear backbone of α (1 → 4)-D-GalA residues. The carboxylic acid groups on the galacturonic chain of pectin are esterified with different numbers of methyl groups, yielding a variety of low (<50 %) and high (>50 %) methyl pectins which have wide applications in food matrices as stabilizer, thickening, gelling, and delivery ingredients (Santos et al., 2020). XG is a natural anionic polysaccharide with a high molecular weight. The primary structure of XG is composed of repeated unit of pentasaccharide including D-mannose, D-glucose, and D-glucuronic acid with a 2:2:1 M ratio. XG exhibits a high solubility, thus, is preferred to be used as suspending, stabilizing, and thickening agent for industrial applications including prepared foods, bakery, and beverages (Abu Elella et al., 2020).

In this study, we hypothesized that long-chain hydrocolloids could form electrostatic interactions between their negatively charged carboxyl groups and Cu^{+2} in SCC, preventing the SCC molecules to be accumulated under acidic conditions followed by their precipitation. Our main goals were: (1) to investigate the effect of hydrocolloids on the stability of SCC in acidic system, (2) characterizing the interactions by FTIR technique, and (3) obtaining a more stable SCC in acidic conditions.

2. Materials and methods

2.1. Materials

PE (galacturonic acid ≥ 74.0 %, average molecular weight, Mw, 485 kDa) from citrus peel (P9135, CAS Number 9000–69-5), CMC (C9481, CAS Number 9004–32-4, Mw ≈ 250 kDa), XG from *Xanthomonas campestris* (G1253, CAS Number 11138–66-2, Mw ≈ 2000 kDa), κ-carrageenan gum (CG, 22048, CAS Number 11114–20-8, Mw 300 kDa), gellan gum (GG, G1910, CAS Number 71010–52-1, Mw ≈ 200–300 kDa), and GA from acacia tree (51198, CAS Number 9000–01-5, Mw ≈ 250 kDa) were purchased from Sigma-Aldrich (USA). Tragacanth gum (TG) was purchased from Titrachem CO. (Tehran, Iran). PS80 (34112170, synthesis grade, Art 822187, Mw 1.31 kDa) was from Merck (Germany). Commercial SCC (purity > 90 %) was purchased from Chr. Hansen (Denmark).

2.2. Preparation of model solutions containing SCC and stabilizers

According to the pre-experiments (1-day storage of acidic solutions containing SCC and different biopolymers in changed levels), the minimum concentrations of ingredients that were apparently successful in stabilizing SCC (CMC 0.012 %, PE 0.024 %, XG 0.004 %, GA 0.01 %, and PS80 0.002 %) were selected to be further evaluated. Stabilizer (PS80 or selected hydrocolloids) were dissolved in distilled water at 80 °C for 30 min (Heidolph Instruments GmbH & Co. KG, MR Hei-Standard, Schwabach, Germany). In the case of PS80, first, a concentration of 2 % (w/v) was prepared as stock solution and then, different amounts were added to the model solution. After dissolution of the stabilizers, sodium citrate (0.1 %, w/v) and SCC (0.003 %, w/v) were added to the solutions, and the pH of samples (WTW, pH 7310, Wellheim, Germany) was reduced to 3.5 (as common pH of fruit juices and drinks) using 200 μL of a citric acid solution (50 % w/v). Next, the solutions were poured into closed bottles. The control sample also contained all above compounds without citric acid and stabilizers. All samples were pasteurized at 90 °C for 1.0 min (Lab water bath, Pars Azma Co., WB10-D, U.M 60, Tehran, Iran).

2.3. Monitoring the samples' stability and their physical properties

Samples that did not precipitate after pasteurization were stored for 28 days at room (25 °C) and accelerated (42 °C in Binder oven, FD 115, Tuttlingen, Germany) temperatures, and their pigment stability (no precipitation) and color features were investigated weekly. The lightness (L^*), redness/ greenness, (a^*) and yellowness/blueness (b^*) indices of the prepared model solutions were determined using a HunterLab (ColorFlex EZ Spectrophotometer, Virginia, USA) colorimeter (Özkan and Bilek, 2015). Particle Size Analyzer instrument (Cordouan Technologies, vasco 3, Photonique, France) was used to measure particle size and polydispersity index (PDI). Zeta-potential (ZP) was determined by a Zetameter (CAD Instruments, ZetaCompact, Naucelle, France).

2.4. Fourier transform infrared (FTIR) spectroscopy

The model solutions (pH = 3.5) containing individual components, namely SCC, sodium citrate, citric acid, hydrocolloids, or PS80, as well as their selected complexes (not precipitated as above-explained) were freeze-dried to be characterized by FTIR, avoiding saturation of spectra by the water associated with the materials (Pereira de Oliveira, et al., 2022; Hosseini and Jafari, 2020). The powders were mixed with KBr and pressed on KBr pellets. The FTIR spectra of samples were analyzed using the Thermo Nicolet (Avatar 370, Lancashire, England) in the mode of transmittance percentage (%T) within the frequency range of 4000–400 cm^{-1} (Abu Elella et al., 2020; Kang et al., 2019; Hosseini et al., 2019).

2.5. Statistical design

To investigate the effect of pasteurization, storage, and the type of stabilizers on the color indices of samples, a completely randomized factorial test was done using SPSS software (version 21). Indeed, mean comparison of particle size and ZP tests were performed in the form of one-factor design at a time, based on Duncan's multiple range test. The tests were performed with at least two replications.

3. Results and discussion

3.1. Physical properties of model solutions containing SCC and stabilizers

SCC pigments were easily dissolved in the drink without citric acid (at neutral pH), but after adding citric acid and pasteurization of the model solutions, the pigments first became suspended particles (not dissolved) in the drink and precipitated in a short time (after 1.0 h), as shown in Fig. 1a, b. Thus, PS80 and hydrocolloids were used to stabilize SCC in acidic conditions.

The results showed that the ratio of 0.67 parts PS80 to 1 part of SCC stabilized SCC in the acidic solutions. PS80 by adsorbing at the interface can prevent SCC molecules from flocculation and eventually precipitation (Nikkonen, 2015). Frost and Saleeb (1999) used PS80 to prepare acid-resistant (pH < 4) SCC and observed that the color of the solution was stable in the SCC-to-PS80 ratios of 1:1 to 1:6. The biopolymers of GG, CG, and TG had no effect on the color stability of SCC in the model solution, so that in a short time, the green pigments were deposited in these samples (data not shown). GA (33.3:1), PE (8:1), CMC (4:1), and XG (1.33:1) stabilized the green SCC in an acidic environment, as the

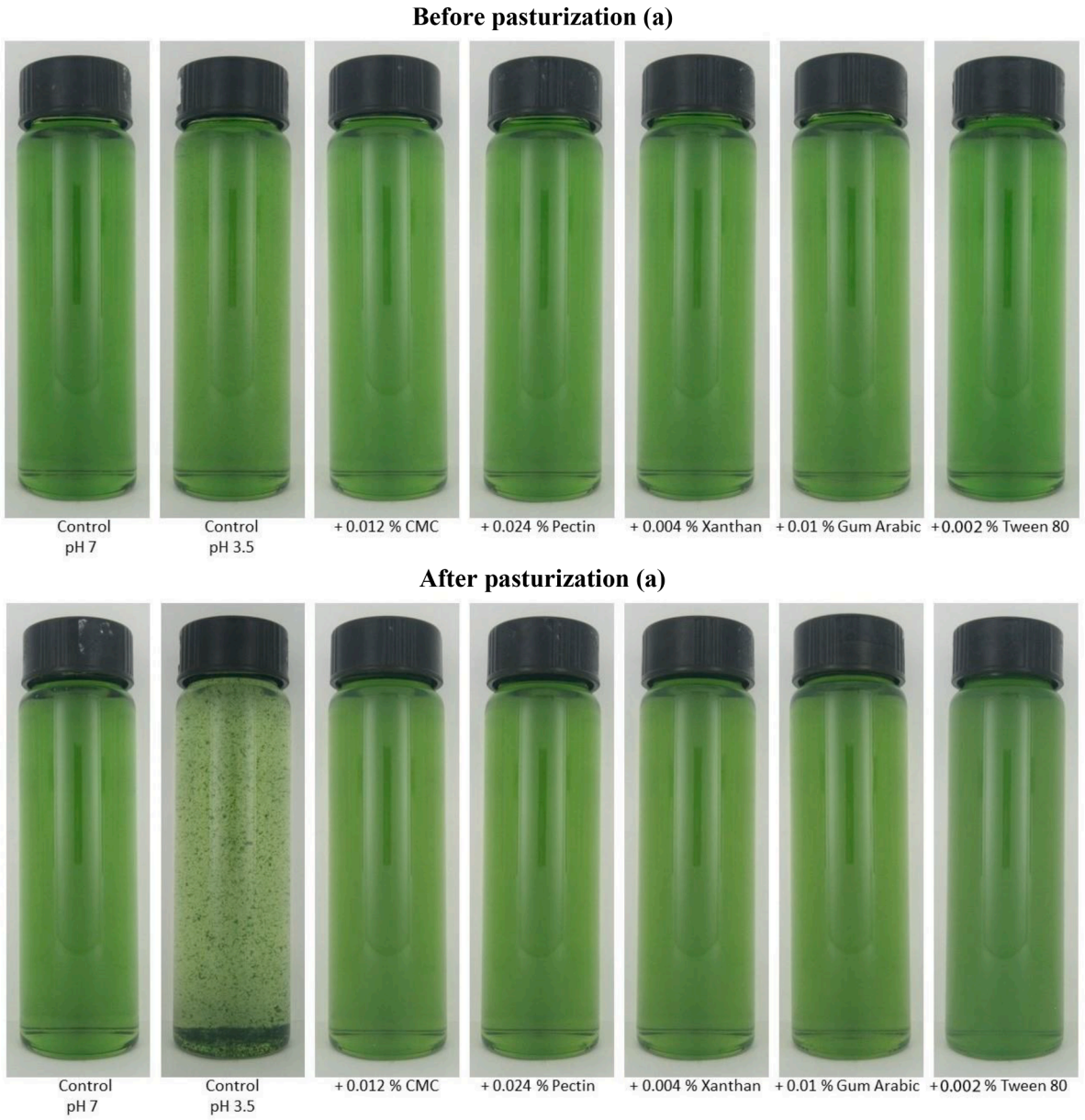

Fig. 1. Images of the model solutions containing sodium copper chlorophyllin (SCC, 0.003 %, w/v) + stabilizers, before (a) and after (b) pasteurization treatment; (c) Average color values for control and stabilizer-containing solutions of SCC at pH = 3.5, as a function of pasteurization treatment and storage period, where values with different letters means significantly different ($P < 0.05$).

samples' color remained stable for 28 days (Fig. 1). Thus, among the hydrocolloids, CMC and XG were the most effective and low-cost stabilizers for the green color of SCC in acidic solutions, so that they provided the desired stability at the lowest concentrations.

Although SCC is a water soluble pigment, it precipitates as soon as the environment becomes acidic, which seems to be a self-assembling phenomenon. In fact, due to the sample's pH $<$ Pk_a of SCCs, the COOH groups of SCCs will be non-ionized, approaching and precipitating each other. On the other hand, at higher pHs, COO^- groups provide a repulsive effect between SCC particles, resulting in a stabilized color. As can be seen in Table 1, even before apparent aggregation of particles in the control sample, its chlorophyllin particle size was significantly larger than that of SCCs stabilized by hydrocolloids or PS80. Thus, by using these stabilizers, the average particle size diminished significantly and prevented the formation of particle complexes and no deposition of particles.

As displayed in Fig. 2, with the addition of either GA, PE, CMC, XG, or PS80, the ZP was significantly reduced ($P < 0.05$), which can cause electrostatic interactions and prevent pigment accumulation, thus stabilizing the pigments in the solution at low pHs. Selig et al. (2020) observed that both XG and sodium alginate significantly increased the negative charge of SCC solutions at both pH = 3 and 5. In the present study, ZP value of the control sample (no stabilizers) at pH = 3.5 was positive (Fig. 2) due to the positive charge of the pigment' copper cation. The associated carboxyl groups of the pigment also became protonated under these conditions. This caused the net charge of SCC to be neutralized in acidic conditions (pH = 3.5) and particle aggregation occurred (Selig et al., 2020). Selig et al. (2020) stated that 0.2 % XG was required for the stability of 0.033 % SCC (i.e. 6 times), while in our study this ratio was 1.33:1 for XG-to-SCC ratio.

Indeed, the ZP value introduces the nature and magnitude of electrostatic charges in the surface of particles as one of the main forces facilitating intermolecular interactions. Further, ZP is considered as a measure of the extent of electrostatic attraction/repulsion between particles (Roque et al., 2009); high values of ZP outside the − 30 mV to + 30 mV interval enhances the repulsive forces prohibiting the aggregation of particles with the same charge sign (Roque et al., 2009; Shaddel et al., 2018). ZP test (Fig. 2) showed that the stabilizers significantly increased the negative charge of SCC solution since they contain carboxylic groups (–COOH ↔ $–COO^-$) as ionizable species. This approach supported by literature, where GA had a negative charge within pH = 2.0–11.8 (Shaddel et al., 2018), and carboxylic acid groups associated with guluronic acids in the side-chains of XG made it highly electronegative with a ZP = -57.2 mV (Cai et al., 2020). However, ZP values of the samples, ranging between + 0.59 for SCC-PS80 to –3.55 mV for SCC-XG, indicated that electrostatic repulsion forces did not play a key role in SCC stabilization. The declined ZP values recorded for SCC solutions in the presence of stabilizers might be due to coating the surface of SCC particles by applied hydrocolloids and existence of electrostatic interactions between them and SCC. Thus, steric repulsion approach explains the mechanism for SCC stabilization as will be further justified by FTIR results.

3.2. The effect of storage conditions on the stability of SCC

Color stability (no precipitation basis) of model drinks containing SCC and XG, CMC, PE, and GA or PS80 stabilizers was evaluated after and pasteurization process (Fig. 1a, b) as well as during storage time (Fig. 1c). The L^* and greenness of samples after pasteurization as well as 4 weeks of storage at 25 and 42 °C, not only decreased but also increased significantly (Fig. 1c). Thus, neither acidic condition nor pasteurization treatment and storage temperature had a negative effect on stabilized SCC, as green color remained stable over time. Note that the storage stability of the model solutions was retained up to 3 months at room temperature when the authors monitored the samples qualitatively/visually (without an apparent change) over long-term storage. However, Selig et al. (2020) observed that the color of acidic solutions stabilized by sodium alginate and XG was changed to olive green color after 5 days of storage at 40 °C, which was due to the removal of copper ions and the phenomenon of pheophytization.

3.3. Influence of stabilizers on the chemical interactions

A mid-range IR spectrum (4000–400 cm^{-1}) was plotted (infrared intensity versus wavenumber or frequency of light) to characterize the molecular composition and structure of materials used to stabilize the SCC in acidic medium, as well as to interpret the possible interactions between the pigment and stabilizers. The graphical FTIR spectra is available in Fig. 3, and the specific frequency of their functional groups is listed in Tables 2 (SCC) and 3.

Based on Fig. 3 and Table 2, the aromatic rings of SCC were identified from vibrations of C—H (1450 and 2953.4 cm^{-1}) and C═C–C (1570.9 cm^{-1}) groups (Coates, 2006). Further, the fingerprint region for SCC showed many other characteristic bands (e.g., vinyl C—H bending and Cu vibrations) as listed in Table 2. All assignments listed in Table 2 for SCC were in accordance with the literature. A broad intensity band at 3417.3 cm^{-1} was recorded for SCC powder, while it can also be reasonably related to an O—H stretching vibration of water traces associated with the potassium bromide (Farag, 2006). The signals observed at low frequencies (820.1 and 922.3 cm^{-1}) for SCC –as seen for other phthalocyanines namely Fe, Pt, Ni, Pd, CO, and Zn– were evidence of the strong bonding between Cu and the four neighboring nitrogen atoms in the pyrrole rings, ensuring the unique stability of the metal phthalocyanine (Farag, 2006).

Broad intensity peaks observed at 3700–3000 cm^{-1} for all ingredients were attributed to O—H stretching and intramolecular or intermolecular H-bonding, as well as N—H stretching mode in the SCC and GA spectra (Table 3). The lower frequencies ($< \sim 3550$ cm^{-1}) within this region are frequently assigned to H-bonded hydroxyls, while the higher ones, in particular as a narrow band > 3600, are due to non-bonded hydroxyl groups (Coates, 2006; Farag, 2006; Nandiyanto et al., 2019). Despite most samples showing a broad band through this region, some ingredients namely buffer components and PE obviously presented several characteristic bands due to dimeric OH stretch (3550–3450 cm^{-1}) and normal "polymeric" OH stretch (~3409 cm^{-1}),

Table 1
Color values and particle size of solutions containing sodium copper chlorophyllin (SCC) + stabilizers at pH = 3.5.

Type of stabilizer	Particle size (Z average) (nm)	Polydispersity index (PDI)	Color features			
			L^*	a^*	b^*	ΔE
Control (pH = 7)	–	–	2.83 ± 0.04^{g}	-2.40 ± 0.06^{e}	1.68 ± 0.27^{b}	–
Control (pH = 3.5)	1462 ± 226^{a}	2.36 ± 0.96^{a}	3.64 ± 0.07^{f}	-2.42 ± 0.06^{e}	0.71 ± 0.08^{de}	1.34 ± 0.04^{f}
Gum Arabic-SCC	464 ± 26^{c}	0.18 ± 0.03^{c}	5.16 ± 0.12^{b}	-3.63 ± 0.13^{b}	1.77 ± 0.15^{c}	2.74 ± 0.04^{b}
Xanthan gum-SCC	605 ± 71^{c}	0.22 ± 0.04^{c}	4.75 ± 0.13^{c}	-3.27 ± 0.07^{c}	0.86 ± 0.07^{d}	2.33 ± 0.1^{c}
CMC-SCC	852 ± 54^{b}	0.92 ± 0.07^{a}	4.17 ± 0.03^{d}	-2.80 ± 0.25^{d}	0.55 ± 0.06^{ef}	1.87 ± 0.01^{d}
Pectin-SCC	703 ± 97^{bc}	0.34 ± 0.11^{bc}	3.80 ± 0.07^{e}	-2.56 ± 0.19^{e}	0.35 ± 0.10^{f}	1.71 ± 0.02^{e}
Polysorbate 80-SCC	196 ± 19^{d}	0.35 ± 0.03^{bc}	6.64 ± 0.03^{a}	-5.45 ± 0.21^{a}	2.44 ± 0.03^{a}	5.43 ± 0.1^{a}

Control was a model solution containing SCC at pH = 7 or 3.5. Values with different letters within columns means significantly different ($P < 0.05$).

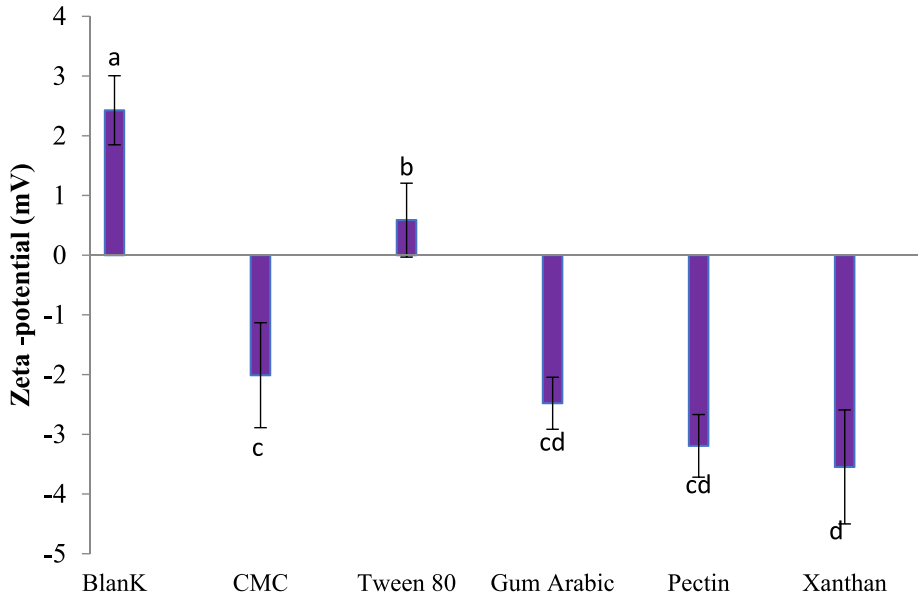

Fig. 2. Zeta-potential values for the model solutions containing sodium copper chlorophyllin + stabilizers at pH = 3.5. Values with different letters means significantly different ($P < 0.05$).

respectively, as they were well distinguished from bands of H-bonded hydroxyls at around 3270 cm^{-1} (Fig. 3). Indeed, in groups such as carboxylic acids which have high tendency to form strong hydrogen bindings, a highly characteristic band can be observed at lower frequencies within O—H absorption region, indicating the formation of a stable dimeric structure (Coates, 2006; Nandiyanto et al., 2019).

Banu and Pavithra (2015) identified and compared the functional groups of chlorophyllin samples extracted from six medicinal plants with the corresponding bands recorded for standard chlorophyllin. They assigned the bands at 1395–1457 cm^{-1} to the aromatic ring of SCC structure which was in agreement with our results (Table 2). Sodium citrate ($Na_3C_6H_6O_7{\cdot}5H_2O$) is derived from citric acid (Bichara et al., 2012), and we used both of them as a buffer system to adjust the pH of SCC-containing solutions. The assignments of buffer components (Fig. 3) are listed in Table 3 with diagnostic bands in the fingerprint region, namely CH_2 twisting and OH torsion modes (Bichara et al., 2012), bending vibration of hydroxyl groups, and skeleton C—H rocking motions (Noerpel and Lenhart, 2015). Other functional groups (>1500 cm^{-1}) of buffer components (Table 3) were also well identified according to the literature (Bichara et al., 2012; Noerpel and Lenhart, 2015).

The fingerprint IR absorption region for hydrocolloid polysaccharides provided good information (Table 3) about their common absorptions at around of 840 cm^{-1} and 1200–1000 cm^{-1} (Mazuki et al., 2020; Santos et al., 2020; Abu Elella et al., 2020), as well as some diagnostic bands at ~ 775 cm^{-1} and 1050–900 cm^{-1} for GA (Gopi et al., 2019), at ~ 916 cm^{-1} for PE (Santos et al., 2020), and at 650–413 cm^{-1} and ~ 1024 cm^{-1} for XG (Saravanan and Subramanian, 2016). PS80 exhibited a number of bands in the fingerprint region (Joshi et al., 2016), in particular the bands appearing at ~ 950 cm^{-1} due to vinyl (CH = CH) C—H out-of-plane bending (Nandiyanto et al., 2019). Furthermore, the group frequencies' region (>1500 cm^{-1}) for these materials was characterized according to previous experiences as listed in Table 3. Intense IR bands of PE in 1150–1000 cm^{-1} (Fig. 3) are attributed to the high content of homogalacturonan in PE (Santos et al., 2020). The average of the peaks of esterified carboxyl group over the sum of signals in esterified and free carboxyl groups is considered as degree of methyl esterification for PE (Santos et al., 2020; Ninčević Grassino et al., 2020). Based on PE spectra, the higher intensity signal at 1744.4 cm^{-1} related to the esterified carboxyl groups in comparison to the one for free carboxyl group (1400–1600 cm^{-1}) confirmed that a high methyl pectin (HMP) was used in the present study. Taking the high polysaccharide-to-glycoprotein ratio into account for GA, the N—H stretching vibration bands (Table 3) were masked by the broad adsorption band from polysaccharide's O—H groups (Roque et al., 2009).

Next, SCC and citrate were added to the stabilizer-containing solutions, followed by adjusting the pH at 3.5 by citric acid. The IR spectra of SCC-stabilized powders were compared with those individually plotted for SCC, sodium citrate, citric acid, and stabilizer powders to determine how SCC flocculation and precipitation in acidic model solution could be prevented. Owing to low pH of buffer, the SCC-buffer IR spectrum (Fig. 3) showed an additional peak at ~1728 cm^{-1} due to $\upsilon_{C=O}$ associated with protonated carboxyl groups (Noerpel and Lenhart, 2015). The peak of buffer components at about 1200 cm^{-1} attributed to C—O—H bending was also dominant at low pH in agreement with the carbonyl stretch, confirming it originated from COOH groups (Noerpel and Lenhart, 2015). According to Fig. 3 and Table 3, the decline in intensity of C═O band of citric acid (~1728 cm^{-1}), related to symmetric (~1395 cm^{-1}) and asymmetric (1592 cm^{-1}) C—O stretches, being in line with reduced intensity of 1214.4 cm^{-1} signal, indicated that a number of their carboxylic acid groups were deprotonated at low pH in the presence of SCC' copper, reflecting an interaction between them (Noerpel and Lenhart, 2015). This would be clearer by considering the changes in Cu (removed) and metal ligand (broadening, reduced wavenumber, and a little reduced intensity) bands (Table 2). Further, the binding between carbonyl groups from SCC and buffer compounds was detected due to reduction in the peak intensities for double bonds (C═C at ~ 1571 and 710 cm^{-1}) or aromatic ring (at ~ 1401 cm^{-1}), and shifting the frequency of citrate carbonyl band (~1667 cm^{-1}) to a lower wavenumber at ~ 1620 cm^{-1} (Nandiyanto et al., 2019), as shown in (Fig. 3).

Fig. 3 also demonstrates the variations in the SCC IR spectra as a function of stabilizer type. To this end, the absorbance peaks related to SCC, as well as their changes in the presence of hydrocolloids and PS80 are listed in Table 2. In general, the recorded spectral changes were due to major interactions (especially, electrostatic types) of the functional groups of stabilizing agents (mostly hydroxyl, carboxyl and PS80 acyl chains) with SCC atoms as briefly discussed below.

It is reported that the contribution of aldehydes, ketones, esters, and carboxylic acids in the interactions can reduce the frequency of carbonyl group absorption (Nandiyanto et al., 2019). The carboxylate C═O signal from stabilizers at about 1630 cm^{-1} disappeared in complex IR spectrum, as a result of their contribution to interactions; in turn, the signal

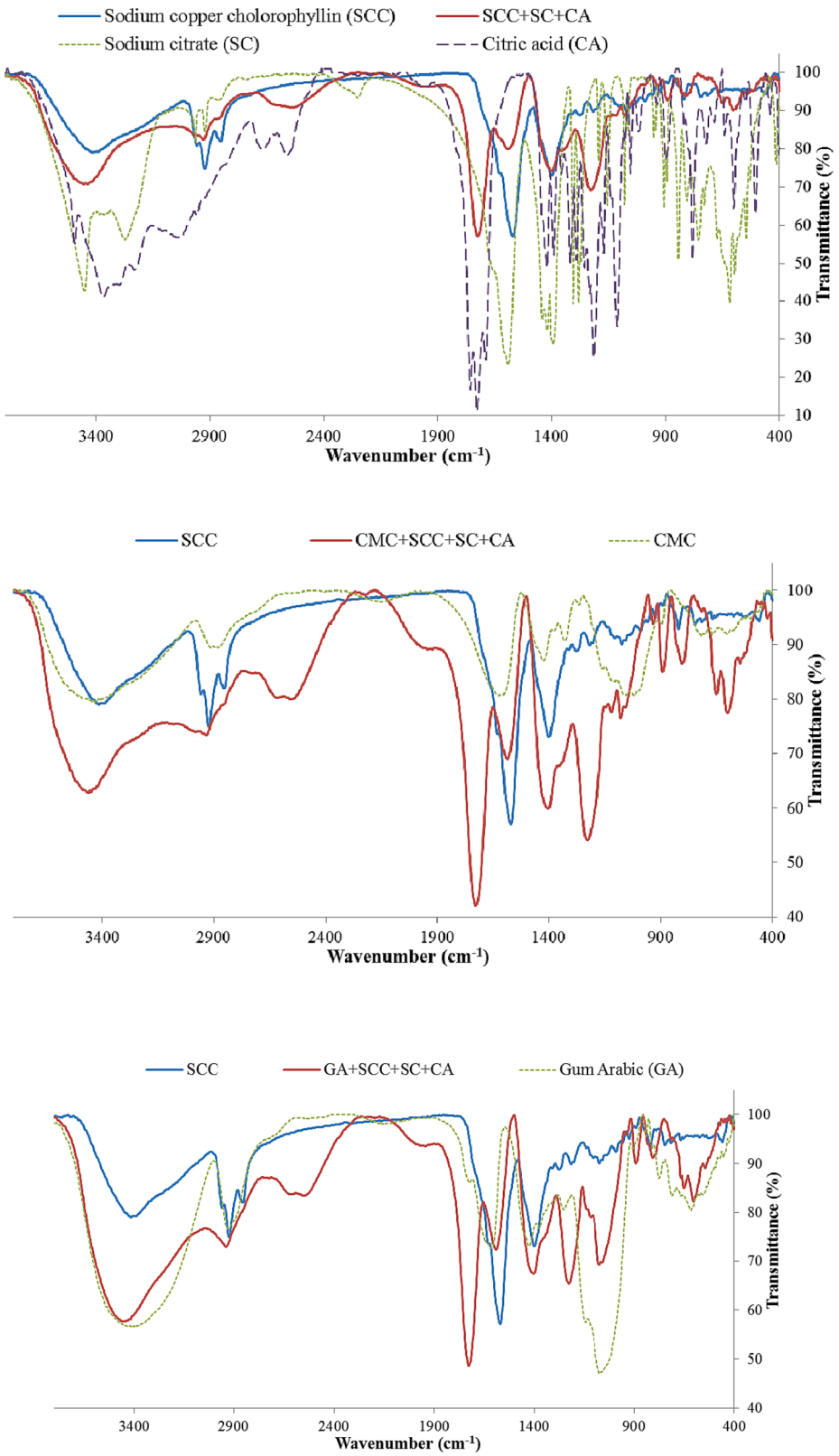

Fig. 3. FTIR spectra of sodium copper chlorophyllin (SCC), sodium citrate, citric acid, hydrocolloids, and polysorbate 80, as well as their complexes at pH = 3.5. The spectra of buffer components were removed from stabilizer-containing samples to enhance visibility.

frequency diminished and overlapped with bands from carboxylate C—O stretching as well as tetrapyrrole system vibrations at around 1580 cm^{-1} (Fig. 3) (Abu Elella et al., 2020). The signal of carboxylate C—O vibration at 1218.5 cm^{-1} for SCC (Fig. 3) was masked by strong peak of citric acid due to carboxylic C—O—H bending at 1214.4 (Banu and Pavithra, 2015; Fronczak et al., 2019). However, the intensity of this

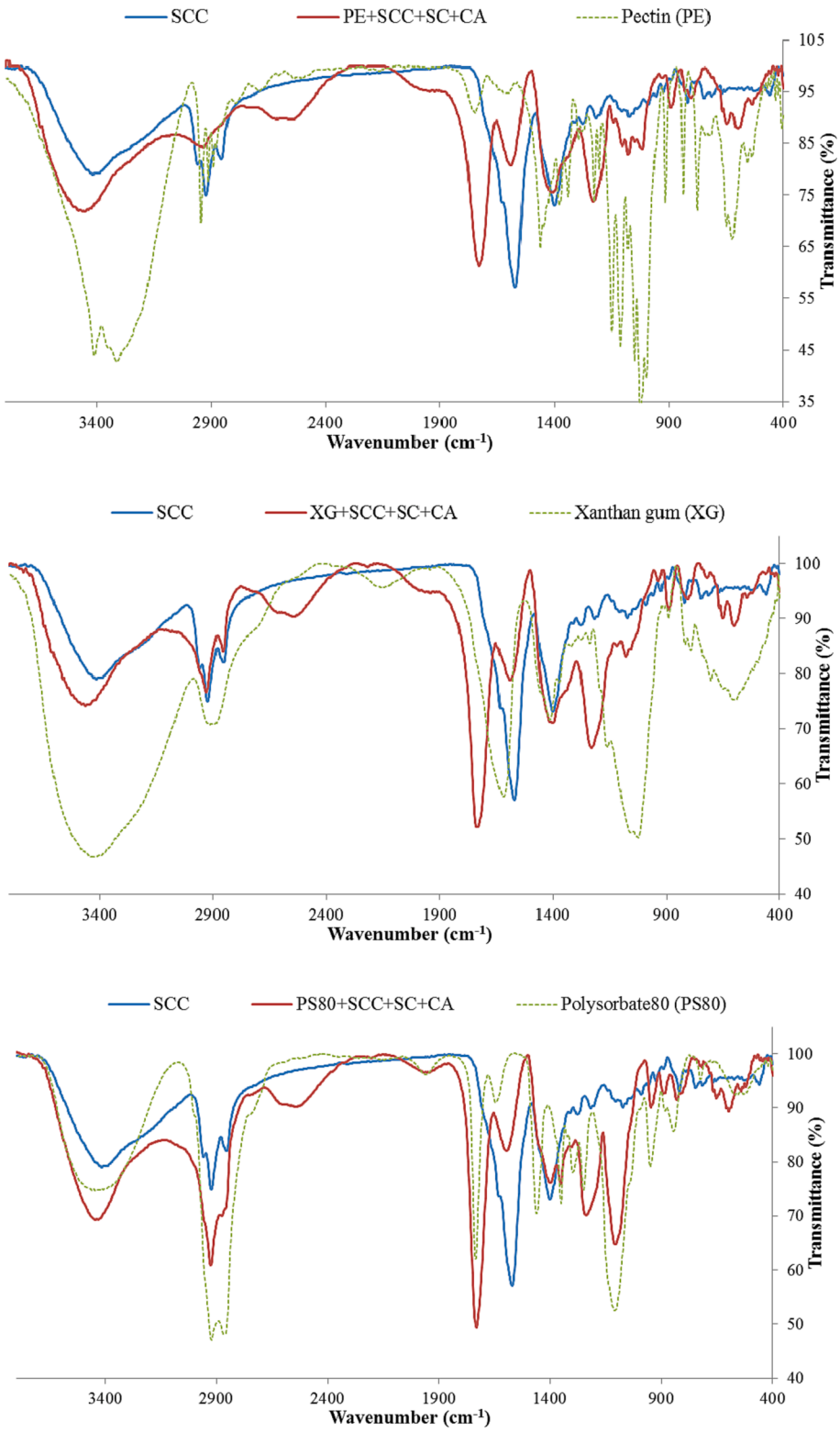

Fig. 3. (*continued*).

band for citric acid was reduced in the presence of other components (Fig. 3), confirming the reduction of COOH concentration in the medium as postulated by reducing the intensity of the strong band of citric acid (1728.7 cm^{-1}), and increasing the intensity of a band at about 2900 cm^{-1} (Fig. 3, Table 3) assigned to free negatively charged carboxyl groups which was not characteristic in citric acid IR spectra (Mansour et al., 2020); however, in the case of PE and PS80 compared to the rest of complexes, weaker and stronger signals at about 2900 cm^{-1} were respectively observed, due to PE structure which was rich in methoxyl groups (i.e., the carboxyl groups conjugated with methyl group), and strong band of PS80 (only contained esterified carboxyl groups) at 2923.3 cm^{-1} related to C—H stretching of $–CH_2$ in acyl chain of fatty acid.

As the contribution of hydroxyl groups to strong hydrogen

Table 2
The changes in FTIR spectra of sodium copper chlorophyllin (SCC) in the absence/presence of the stabilizers at pH = 3.5.

Wavenumber (cm^{-1})	Origin *	Changes of wavenumbers (cm^{-1})					
		SCC	+ CMC	+ Gum Arabic	+ Pectin	+ Xanthan Gum	+ PS80
710 or 746.57	Metal atom (Cu), 750–570	Removed	711 Re or removed	711 Re or removed	702 Re or removed	722.8 Re or removed	722 Re or removed
820.1	Metal ligand (M–N)	815.7 Br, Lre	804.6 Br, In	806.2 Br, In	803.9 Re	806.2 Br	804.1 Br
922.3	Metal ligand (M–N)	935.3 Lre	933.9 Lin	931 Lre	925 Re	939.4 Re	946.7 In
950	Vinyl C—H out-of-plane bend	Removed	Removed	Removed	Removed	Removed	Masked
987.7	C—H (963–1077), C—C stretching and bending vibrations in the pyrrole ring (922–988)	Removed	Overlap	Overlap	Overlap	Removed	Removed
1073.7	C═O C—O stretching vibrations	1080.6 Lin	1079.5 In	1076 In	1077.7 In	1079.2 In	Overlapped
1218.5	COO^- (1058–1238), skeletal C—C vibrations, or aromatic C—H in-plane bend, stretching vibrations of C—O—C ester bonds	1229.2 In, Br	1227.2 In, Br	1228.3 In, Br	1230.3 In, Br	1231.0 In, Br	1237.7 In, Br
1273.8	Stretching mode of C-17[3]–O and C-13[3]–O in ester groups C—N stretching vibrations	Overlap	Overlap	Overlap	Overlap	Overlap	Overlap
1400.9	Aromatic ring (1395–1457 and C—O stretching vibrations	1380 Lre	1403.6 In	1405.3 In	1415.6 Re	1402.9 Br, In	1398.1 Re
1570.9	C═C and C═N in the highly conjugated system of tetrapyrrole system	1591.4 Re	1586.1 Re	1592.4 Re	1591.6 Re	1590.8 Re	1593.8 Re
~1620 shoulder	Stretching mode of the aldehyde or carboxylate carbonyl group	~1620 Re	Disappeared	Disappeared	Disappeared	Disappeared	Disappeared
2854.8 shoulder	C—H stretching of aldehyde group	2852 Re	2848 Lin, Br	Lin, Br	Removed	2856.4 Lre	2872.2 In
2923.8	C—H stretching of the methyl, methylene, or methine group in phytol	2930.7 Re	2936.1 Lin, Br	2928.3 Lin, Br	2936.2 Re, Br	2929.4 Lre	2926.1 In, Br
2953.4 shoulder	Asymmetric C—H stretching mode of the $–CH_3$ group	2960 Re	Masked	Masked	Disappeared	Disappeared	Masked
3417.3 (~300–3680)	O—H and N—H stretching mode	3455.3 (~2990–3733) In, Br	3463.1 (~3000–3750) In, Br	3450.6 (~3027—3770) In, Br	3450.8 (~3050–3700) In, Br	3462.7 (~3000–3695) In, Br	3446.8 (~3000–3690) In

SCC: Sodium copper cholorophyllin, SC: Sodium citrate, CA: Citric acid, SCS: SCC + CA + SC, CMC: Carboxymethyl cellulose, GA: Gum Arabic, PE: Pectin, XG: Xanthan gum, PS80: Polysorbate 80/Tween 80, Re: Reduced intensity, In: Increased intensity, Lre/in: Little reduced/increased intensity, Br: Broadened band.
* References: Farag, 2006; Nandiyanto et al., 2019; Banu & Pavithra, 2015; Fronczak et al., 2019; Coates, 2006; Kang et al., 2019; Norman et al., 2016;Siwińska-Ciesielczyk et al., 2019.

interactions was increased, it was expected that the mean absorption frequencies within the O—H stretching frequency zone (3700–3200 cm^{-1}) would be broadened significantly, more intense and shifting to the lower frequencies as a function of the strength and degree of the hydrogen bonds (Coates, 2006; Kareem Ahmed et al., 2015). Considering the O—H frequency region in Fig. 3, the IR peak of SCC at pH = 3.5 in the presence/absence of stabilizers was more intense (especially with CMC, GA, and PS80) and shifted to the higher frequencies, indicating that its contribution to the weakly hydrogen bonded structures was enhanced (Gerola et al., 2019). Also, Fig. 3 confirmed that the new formed H-bonds were mostly intermolecular type compared to original ones as can be found from increased O—H frequencies (Coates, 2006). Nevertheless, the increase in intensity and area of O—H bands (Fig. 3) was also due to the dominance of protonated carboxyl groups in the structure of involved molecules when the pH value reached 3.5.

The intensity of citric acid band at 2615 cm^{-1} was reduced in the presence of other substances (in particular for SCC, SCC-PS80, SCC-XG and SCC-PE,), indicating that the dimeric carboxylic acids were reduced (Coates, 2006). Monitoring the C—O vibrations of COO^- of citrate (1592.3 and 1394.6 cm^{-1} bands) in all mixtures, except PS80, demonstrated the contribution of this functional group to the interactions, as can be found from the reduced frequencies, mostly for SCC-CMC (1586.1 cm^{-1}) and SCC-XG (1590.8 cm^{-1}) complexes (Table 2). Further, the frequency changes of these hydrocolloids (Table 3) confirmed that the hydrogen interactions in the model systems were increased. Thus, the FTIR analysis showed that the occurrence of significant interactions between SCC and the well-distributed stabilizers (especially PS80, XG and CMC) led to a considerable reduction in SCC particle size (Deloye et al., 2017), improving the SCC distribution within acidic environment (Supplementary Materials). Furthermore, the negative charges associated with hydrocolloids (justified from bands at 2900 and 1600–1400 cm^{-1}) partially contributed to stabilization of the pigment in such system via repulsion effects as discussed in the results of ZP.

It was confirmed that the primary role of PS80, as an emulsifier, for producing a stable pigment in aqueous medium was mainly due to acting as a guard for hydrophobic sites on the pigment surfaces, which are prone to intermolecular cross-linking and aggregation of pigments, or to inhibition of self-association of pigments by competing with the air–water interface as reported for protein-PS20/80 complexes (Grabarek et al., 2020). This would be confirmed from changes in IR spectra of SCC and PS80 mixture. The metal-related band for SCC-PS80 was weaker than for SCC-hydrocolloids due to masking the functional group by acyl chain of PS80 polymer when its ether moieties contributed to the electrostatic interactions with CU^{2+} in the SCC structure as confirmed by changes observed in the frequency and intensity of IR bands in PS80 (845.8, 1045 and 1109.1 cm^{-1}) and SCC (metal related bands). It can also be justified from comparing the ZP values for SCC solutions (pH = 3.5) in the presence and absence of uncharged PS80 surfactant (Fig. 2), as SCC-PS80 complex significantly showed a lower positive charge than other one.

Considering the PS IR spectrum in SCC-SP FTIR, reduction in intensity and shift of C—H (CH = CH) out-of-plane bending band (950.3 to 946.6 cm^{-1}), disappeared (1045 cm^{-1}) and reduced intensity (1109.12 cm^{-1}) C—O—C peaks, disappeared asymmetric carbonyl stretch band (1644.13 cm^{-1}) and elevation of frequencies from 2864.0 cm^{-1} (acyl chain $–CH_2$) to 2872.19 cm^{-1} as well as from 2923.3 cm^{-1} (acyl chain $–CH_3$) to 2926.1 cm^{-1} –due to restriction in acyl chain fluidity arising from hydrophobic interactions (Joshi et al., 2016)– for PS, revealed that hydrophobic moiety of PS80 was mainly directed toward SCC. On the other hand, its hydrophilic fraction mostly contributed to hydrogen interactions with surrounding polar matrix, as confirmed by some evidences, including disappeared C—O (ethylene oxide) band (1460.6 cm^{-1}) of PS80, carbonyl peak shifting from 1735.1 to 1731.9 cm^{-1} (a measure of the degree of PS80 hydration (Joshi et al., 2016)), and increased intensity plus broadened O—H band for both SCC and PS80.

Table 3
FTIR spectra of buffer and stabilizers in the presence of sodium copper chlorophyllin (SCC) at pH = 3.5.

Peak assignment	Wavenumber (cm^{-1}) of components (original / affected by SCC)						
	Sodium citrate (1)*	Citric acid (1)	CMC (2)	Gum Arabic (3)	Pectin (4)	Xanthan Gum (5)	Polysorbate 80 (6)
Skeletal mode vibrations of the pyranose rings	–	–	–	400–700 / Re, LW	–	–	–
C–C═O in-plane bending	–	–	–	–	–	468 and 413 / Removed	–
CH_2 twisting modes	412.3 / Removed	–	–	–	–	–	–
OH torsion modes	528.5 / Re or Removed	–	–	–	–	–	–
CH_2 twisting modes	547.3 / Re or Removed	–	–	–	–	–	–
O–CO in-plane bending	–	–	–	–	–	591.2 (400–830) / 599.4 Re and 650 / 651.3 Re	–
1–4 linkage of galactose and 1–6 linkage of mannose	–	–	–	775.0 / Overlap, Re	–	–	–
C—O of epoxy rings	–	–	894.4 / 891.67 In	840.1 / 835 Lin and 902.6 / 890.8 In	838.4 / 827 Re	820.9 / 806.2 Re	845.8 / Removed
Skeletal C—C stretching and bending	755.6–945 / Re	722.8 – 935 / Re	1016.9 / Re	710.56 / 711 Re	775.8 / 803.9 Re or Removed	820.9 / 806.2 Re	722.8 / 722 Lre
Carboxylate ion bending	843.8 / removed and 907.7 / 891.6 Re or Removed	–	–	–	–	–	–
The degree of methyl esterification	–	–	–	–	915.8 / 892.2 Re or Removed	–	–
Polysaccharides fingerprint region	–	–	–	900–1050 (arabinogalactan) / Re, LW	950–1200 (glycosidic bonds and pyranoid rings) / Re, LW	–	–
Vinyl C—H out-of-plane bending	–	–	–	–	–	–	950.3 (CH = CH) / 946.65 Re
C—C stretching			1262.2 weak / Masked	–	–	–	
Skeleton C—H rocking motions	1271.4 / Removed and 1419.6 / 1355 Re	1291.2 / Removed	–	–	–	–	
Skeleton C—H rocking of the CH_2	1305.6 / Re	1319.1 / Re	–	–	–	–	
C—H bending		–	–	–	–	1368.4 / Overlap	1350.9 / 1352.2 Lre
C—H stretching	2970.3 / Lre, 2925.3 (In phase CH_2) / 2930.7 Lin and 2864.0 (out of phase CH_2) / 2860 In	2669.0 / 2615 Re and 3040.5 / Removed	2914.0 / 2936.1 Overlap	3000–2800 / Br, Lin	2895, 2913.6 and 2944.2 / 2936.2 Br, Re	2915.1 aliphatic (aldehyde, CH_2 or CH_3) / Removed	2864.0 ($-CH_2$) / 2872.2 Re and 2923.3 ($-CH_3$) (acyl chain of fatty acid) / 2926.1 Re
C—H bending mode of the $-CH_3$	–	–		1380.7 symmetric / 1350 In	1381 symmetric / Disappeared	–	–
Acetal groups bending	–	–		–	–	1024.0 strong (–C–OH) / 1050 Re	–
C—O—C and secondary alcohol C–OH stretching	1079.3 (C–OH) / 1080.6 Re	–	1328.9 (C—O—C) / 1350 In and 1057.8 ($R–CH_2OCOO^-$) CH–O–CH_2 / Lin	1071.5 (asymmetric –C—O—C) / 1076 LW, Re	1024.4 / 1017.0 Re, 1225.2 (saccharide C—O—C), and 1149.9 (glycosidic linkages C—O—C) / 1143 Re	1057.9 (glycosidic ether bond C—O—C) / 1079.2 LW, Re	1045 –C—O of ethoxy (C—O—C) moiety / 1024 Re
C—O stretching	1157.1 (COO^-) / Removed	–	1106.9 ($R–CH_2OCOO^-$) / 1116 In	–	–	1156.0 (C—O—C glycosidic ether bond) / Disappeared	1109.1 (C—O—C ethoxy moiety) / 1108.58 Re
C—O—H bending	1200 (COOH) / Overlap, 1282.6 / Disappeared and 1419.6–1425 (hydroxyl group) / 1345 Re	1214.4 (COOH) / 1229.17 Re	–	–	–	–	–
Symmetric C—O stretching vibrations of COO^-	1394.6 / 1345 Re	1392.4 / 1345 Re	1426.6 / 1403.59 Br, In	1428.0 / 1405.32 Br, In	1460.5 / ~1454 Re	1414.9 / 1402.93, Br	–

(*continued on next page*)

Table 3 (*continued*)

Peak assignment	Wavenumber (cm^{-1}) of components (original / affected by SCC)						
	Sodium citrate (1)*	Citric acid (1)	CMC (2)	Gum Arabic (3)	Pectin (4)	Xanthan Gum (5)	Polysorbate 80 (6)
Asymmetric C—O stretching vibrations of COO^-	1592.3 / 1591.4 Re	–	–	–	–	–	–
OH-bending from water molecules, asymmetric C═O stretch and N—H bending	1666.7 (COO^- C═O) / 1620 Re	1690.2 (COO^- C═O) / 1620 Re	1625.1 (COO^- C═O) / 1586.1 In	1612.2 (COO^- C═O and N—H bending) / 1592.4	1605.5 (COO^- C═O) / 1591.61 In	1619.6 (COO^- C═O and acetate) / 1590.8 LW, Re	1644.1C = O / 1593.8 Br, In
Symmetric C═O stretching of the uncharged carboxylic acid	–	1728.7 (COOH) / 1725.4 LW, Re	–	1728.0 (COOH) / 1728.3 Br, In	1744.4 (methyl ester of carboxylic acid) / 1729.7 Br, In	–	1735.1 (ester moiety)/ 1731.9 Br, In
Free carboxyl groups negatively charged	2925.3 / 2930.7 Lin		2913.9 / 2936.1 Br, In	2928.3 / 2940.56 Br, In	2913.6 / 2936.2 Br, Re	2915.1 / 2929.4 LW, Re	–
O—H stretching (H-bonded hydroxyls)	3274.8 / Re or Removed	3227.7 and 3293.1 / Re or Removed	–	–	3311.4 / Re or Removed	–	–
O—H stretching, and intermolecular or intramolecular H-bonding	3452.5 / 3455.3 Re	3369.7 and 3495.6 / 3455.3 Re	3429.6 / 3463.1 Br, In	3394.4 / 3450.6 LW	3410.4 / 3450.9 LW, Re	3420.1 / 3463.0 LW, Re	3443.7 / 3446.8 In
N—H stretch	–	–	–	3310–3350 secondary amine, 3400–3500 primary amine	–	–	–

SCC: Sodium copper cholorophyllin, Re: Reduced intensity, In: Increased intensity, Lre/in: Little reduced/increased intensity, Br: Broadened band.
*References: (1) Noerpel & Lenhart, 2015; Bichara et al., 2012; Sritham & Gunasekaran, 2017. (2) Mazuki et al., 2020; Jeong et al., 2020; (3) Mazuki et al., 2020; Gopi et al., 2019; Mansour et al., 2020; Banerjee & Chen, 2007. (4) Santos et al., 2020; Ninčević Grassino et al., 2020; Hosseini et al., 2019. (5) Coates, 2006; Abu Elella et al., 2020; Saravanan & Subramanian, 2016; Kura et al., 2014. (6) Coates, 2006; Joshi et al., 2016; Kura et al., 2014; Roacho-Pérez et al., 2020.

Meanwhile, elevation of the frequency for O—H bands of both SCC (3417.3 cm^{-1}) and PS80 (3443.7 cm^{-1}) to 3446.8 cm^{-1} in the complex spectrum supports the increase in dispersion of the components within aqueous medium (shifting from strong intramolecular H-bindings toward weak intermolecular ones with surrounding water).

4. Conclusion

The lowest amount of stabilizer required for the stability of SCC pigment in the model solution was related to PS80, followed by XG and CMC. The use of any of the stabilizers reduced the particle size of SCC and the ZP, which can cause electrostatic interactions thus preventing the accumulation of pigment in the solution at pH = 3.5 for 28 days (up to 3 months, as visual record). The FTIR analysis indicated that the considerable interactions (mostly electrostatic and hydrogen bonds) between SCC and the well-distributed stabilizers led to a considerable decline in SCC particle size, improving the SCC distribution and stability within acidic environment. The primary role of PS80 mainly involved functioning as a guard for hydrophobic sites on the pigment surfaces which are prone to intermolecular cross-linking and aggregation of pigments. Thus, in addition to PS80 surfactant, XG and CMC are the most effective and cost-effective ingredients for the stabilization of SCC green color in acidic solutions, namely beverages, fruit drinks, etc. Further studies are suggested to investigate the other available ingredients, especially modified starches, with economic efficiency, followed by their incorporation into real food systems, and characterization of possible interactions between food ingredients and stabilized SCC using high-tech instruments during shelf life. Moreover, FTIR analysis of the solutions rather than their freeze-dried forms using a FTIR instrument equipped with related tools may be useful for better understanding what happens within the stabilized solutions.

CRediT authorship contribution statement

Hamed Hosseini: Conceptualization, Methodology, Data curation, Investigation, Writing – original draft, Writing – review & editing. **Vahid Pasban Noghabi:** Investigation, Writing – review & editing. **Hamed Saberian:** Methodology, Data curation, Investigation, Supervision, Writing – original draft, Writing – review & editing. **Seid Mahdi Jafari:** Methodology, Supervision, Writing – review & editing.

Declaration of Competing Interest

The authors declare that they have no known competing financial interests or personal relationships that could have appeared to influence the work reported in this paper.

Data availability

The data that has been used is confidential.

Acknowledgment

This work was supported by the Academic Centre for Education, Culture and Research (ACECR), Mashhad, Iran (Grant number 6010–20). Last author acknowledges the Chinese Ministry of Science and Technology "Belt and Road" Innovative Talent Exchange Foreign Expert Project (Grant Number DL2023003001L).

Appendix A. Supplementary data

Supplementary data to this article can be found online at https://doi.org/10.1016/j.fochx.2023.101020.

References

Abu Elella, M. H., Sabaa, M., Hanna, D. H., Abdel-Aziz, M. M., & Mohamed, R. R. (2020). Antimicrobial pH-sensitive protein carrier based on modified xanthan gum. *Journal of Drug Delivery Science and Technology, 57*, Article 101673.
Banerjee, S. S., & Chen, D.-H. (2007). Fast removal of copper ions by gum Arabic modified magnetic nano-adsorbent. *Journal of Hazardous Materials, 147*(3), 792–799.

Banu, N., & Pavithra, S. (2015). A study of chlorophyllin of medicinal plants, its chemical characterization and anti–proliferative activity with special reference to *solanum trilobatum* L. on liver cell line. *International. Journal of Pharmacy and Pharmaceutical Sciences, 7*(12), 69–79.

Bichara, L. C., Fiori Bimbi, M. V., Gervasi, C. A., Alvarez, P. E., & Brandán, S. A. (2012). Evidences of the formation of a tin(IV) complex in citric-citrate buffer solution: A study based on voltammetric, FTIR and ab initio calculations. *Journal of Molecular Structure, 1008*, 95–101.

Cai, X., Du, X., Zhu, G., & Cao, C. (2020). Induction effect of NaCl on the formation and stability of emulsions stabilized by carboxymethyl starch/xanthan gum combinations. *Food Hydrocolloids, 105*, Article 105776.

Coates, J. (2006). Interpretation of infrared spectra: A practical approach. In R. A. Meyers, & M. L. McKelvy (Eds.), *Encyclopedia of analytical chemistry*. John Wiley & Sons.

Deloye, C. J., Lepkowicz, R. S., West, M. S., & Euliss, G. W. (2017). *Variations in Infrared Spectroscopic Signatures*. U.S. Government: The MITRE Corporation.

Farag, A. A. M. (2006). Optical absorption of sodium copper chlorophyllin thin films in UV–Vis–NIR region. *Spectrochimica Acta Part A: Molecular and Biomolecular Spectroscopy, 65*(3), 667–672.

Fronczak, M., Pyrzyńska, K., Bhattarai, A., Pietrowski, P., & Bystrzejewski, M. (2019). Improved adsorption performance of activated carbon covalently functionalised with sulphur-containing ligands in the removal of cadmium from aqueous solutions. *International Journal of Environmental Science and Technology, 16*(12), 7921–7932.

Frost, J. R., & Saleeb, F. Z. (1999). *U.S. Patent No. 5,993,880*. Washington, DC: U.S. Patent and Trademark Office.

Gerola, A. P., Costa, P. F. A., de Morais, F. A. P., Tsubone, T. M., Caleare, A. O., Nakamura, C. V., … Hioka, N. (2019). Liposome and polymeric micelle-based delivery systems for chlorophylls: Photodamage effects on Staphylococcus aureus. *Colloids and Surfaces B: Biointerfaces, 177*, 487–495.

Gopi, S., Amalraj, A., Kalarikkal, N., Zhang, J., Thomas, S., & Guo, Q. (2019). Preparation and characterization of nanocomposite films based on gum Arabic, maltodextrin and polyethylene glycol reinforced with turmeric nanofiber isolated from turmeric spent. *Materials Science and Engineering: C, 97*, 723–729.

Grabarek, A. D., Bozic, U., Rousel, J., Menzen, T., Kranz, W., Wuchner, K., … Hawe, A. (2020). What makes polysorbate functional? Impact of polysorbate 80 grade and quality on IgG stability during mechanical stress. *Journal of Pharmaceutical Sciences, 109*(1), 871–880.

Hosseini, H., & Jafari, S. M. (2020). Chapter Eleven - Fourier transform infrared (FT-IR) spectroscopy of nanoencapsulated food ingredients. In S. M. Jafari (Ed.), *Characterization of Nanoencapsulated Food Ingredients* (vol. 4, pp. 347–410). Academic Press.

Hosseini, S. S., Khodaiyan, F., Kazemi, M., & Najari, Z. (2019). Optimization and characterization of pectin extracted from sour orange peel by ultrasound assisted method. *International Journal of Biological Macromolecules, 125*, 621–629.

Jeong, D., Kim, C., Kim, Y., & Jung, S. (2020). Dual crosslinked carboxymethyl cellulose/polyacrylamide interpenetrating hydrogels with highly enhanced mechanical strength and superabsorbent properties. *European Polymer Journal, 127*, Article 109586.

Joshi, A. S., Gahane, A., & Thakur, A. K. (2016). Deciphering the mechanism and structural features of polysorbate 80 during adsorption on PLGA nanoparticles by attenuated total reflectance-Fourier transform infrared spectroscopy. *RSC Advances, 6*(110), 108545–108557.

Kang, Y.-R., Lee, Y.-K., Kim, Y. J., & Chang, Y. H. (2019). Characterization and storage stability of chlorophylls microencapsulated in different combination of gum Arabic and maltodextrin. *Food Chemistry, 272*, 337–346.

Kareem Ahmed, J., Abdul Amer, Z. J., & Mohammed Al-Bahate, M. J. (2015). Effect of chlorophyll and anthocyanin on the secondary bonds of poly vinyl chloride (PVC). *International Journal of Materials Science and Applications. Special Issue: Steel and Direct Reduced Iron (sponge Iron) Industry, 4*(2-1), 21–29.

Koca, N., Karadeniz, F., & Burdurlu, H. (2007). Effects of pH on chlorophyll degradation and colour loss in blanched green peas. *Food Chemistry, 100*, 609–615.

Kura, A. U., Hussein-Al-Ali, S. H., Hussein, M. Z., & Fakurazi, S. (2014). Preparation of tween 80-zn/AL-levodopa-layered double hydroxides nanocomposite for drug delivery system. *The Scientific World Journal, 2014*, Article 104246.

Mansour, M., Salah, M., & Xu, X. (2020). Effect of microencapsulation using soy protein isolate and gum Arabic as wall material on red raspberry anthocyanin stability, characterization, and simulated gastrointestinal conditions. *Ultrasonics Sonochemistry, 63*, Article 104927.

Mazuki, N. F., Abdul Majeed, A. P. P., Nagao, Y., & Samsudin, A. S. (2020). Studies on ionics conduction properties of modification CMC-PVA based polymer blend electrolytes via impedance approach. *Polymer Testing, 81*, Article 106234.

Nandiyanto, A. B. D., Oktiani, R., & Ragadhita, R. (2019). How to read and interpret FTIR spectroscope of organic material. *Indonesian Journal of Science & Technology, 4*(1), 22.

Nikkonen, T. (2015). *Structure-property relationships and self-assembly of chlorophyll derivatives in development of light-harvesting structures and materials*. Helsinki: Helsingin yliopisto, (http://urn.fi/URN:ISBN:978-951-51-0953-8).

Ninčević Grassino, A., Ostojić, J., Miletić, V., Djaković, S., Bosiljkov, T., Zorić, Z., … Brnčić, M. (2020). Application of high hydrostatic pressure and ultrasound-assisted extractions as a novel approach for pectin and polyphenols recovery from tomato peel waste. *Innovative Food Science & Emerging Technologies, 64*, Article 102424.

Noerpel, M. R., & Lenhart, J. J. (2015). The impact of particle size on the adsorption of citrate to hematite. *Journal of Colloid and Interface Science, 460*, 36–46.

Norman, M., Bartczak, P., Zdarta, J., Tomala, W., Żurańska, B., Dobrowolska, A., … Jesionowski, T. (2016). Sodium copper chlorophyllin immobilization onto *hippospongia communis* marine demosponge skeleton and its antibacterial activity. *International Journal of Molecular Sciences, 17*(10), 1564.

Özkan, G., & Bilek, S. E. (2015). Enzyme-assisted extraction of stabilized chlorophyll from spinach. *Food chemistry, 176*, 152–157.

Pereira de Oliveira, J., Almeida, O. P., Campelo, P. H., de Oliveira Ferreira Rocha, L., Santos, J. H. P. M., & Gomes da Costa, J. M. (2022). Tailoring the physicochemical properties of freeze-dried buriti oil microparticles by combining inulin and gum Arabic as encapsulation agents. *LWT, 161*, Article 113372.

Roacho-Pérez, J. A., Ruiz-Hernandez, F. G., Chapa-Gonzalez, C., Martínez-Rodríguez, H. G., Flores-Urquizo, I. A., Pedroza-Montoya, F. E., … Sánchez-Domínguez, C. N. (2020). Magnetite Nanoparticles Coated with PEG 3350-Tween 80. In Vitro Characterization Using Primary Cell Cultures. *Polymers, 12*(2), 300.

Roque, A. C. A., Bicho, A., Batalha, I. L., Cardoso, A. S., & Hussain, A. (2009). Biocompatible and bioactive gum Arabic coated iron oxide magnetic nanoparticles. *Journal of Biotechnology, 144*(4), 313–320.

Santos, E. E., Amaro, R. C., Bustamante, C. C. C., Guerra, M. H. A., Soares, L. C., & Froes, R. E. S. (2020). Extraction of pectin from agroindustrial residue with an ecofriendly solvent: Use of FTIR and chemometrics to differentiate pectins according to degree of methyl esterification. *Food Hydrocolloids, 107*, Article 105921.

Saravanan, L., & Subramanian, S. (2016). Surface chemical properties and selective flocculation studies on alumina and silica suspensions in the presence of xanthan gum. *Minerals Engineering, 98*, 213–222.

Schwartzberg, L. S., & Navari, R. M. (2018). Safety of polysorbate 80 in the oncology setting. *Advances in Therapy, 35*(6), 754–767.

Selig, M. J., Gamaleldin, S., Celli, G. B., Marchuk, M. A., Smilgies, D. M., & Abbaspourrad, A. (2020). The stabilization of food grade copper-chlorophyllin in low pH solutions through association with anionic polysaccharides. *Food Hydrocolloids, 98*, Article 105255.

Shaddel, R., Hesari, J., Azadmard-Damirchi, S., Hamishehkar, H., Fathi-Achachlouei, B., & Huang, Q. (2018). Use of gelatin and gum Arabic for encapsulation of black raspberry anthocyanins by complex coacervation. *International Journal of Biological Macromolecules, 107*, 1800–1810.

Siwińska-Ciesielczyk, K., Bartlewicz, O., Bartczak, P., Piasecki, A., & Jesionowski, T. (2019). Functional titania-silica/chlorophyllin hybrids: Design, fabrication, comprehensive physicochemical characteristic and photocatalytic test. *Adsorption, 25*(3), 485–499.

Sritham, E., & Gunasekaran, S. (2017). FTIR spectroscopic evaluation of sucrose-maltodextrin-sodium citrate bioglass. *Food Hydrocolloids, 70*, 371–382.

Tumolo, T., & Lanfer-Marquez, U. M. (2012). Copper chlorophyllin: A food colorant with bioactive properties? *Food Research International, 46*(2), 451–459.